3D Motion Estimation Using a Combination of Correlation and Variational Methods for PIV

L. Alvarez, C.A. Castaño, M. García, K. Krissian, L. Mazorra, A. Salgado, and J. Sánchez

Departamento de Informática y Sistemas, Universidad de Las Palmas de Gran Canaria, Campus de Tafira s/n, 35017 Las Palmas de Gran Canaria, Spain
{lalvarez,ccastano,mgarcia,krissian,lmazorra, asalgado,jsanchez}@dis.ulpgc.es

Abstract. Estimation of motion has many applications in fluid analysis. Lots of work has been carried out using Particle Image Velocimetry to design experiments which capture and measure the flow motion using 2D images. Recent technological advances allow capturing 3D PIV image sequences of moving particles. In this context, we propose a 3D motion estimation technique based on the combination of an iterative cross-correlation technique and a variational (energy-based) technique. The performance of the proposed technique is measured and illustrated using numerical simulations.

1 Introduction

"Particle Image Velocimetry (PIV) is a technique which allows one to record images of large parts of flow fields in a variety of applications in gaseous and liquid media and to extract the velocity information out of these images" [6]. Once the flow motion has been captured, software tools are needed to evaluate and display the flow motion.

In this paper, we propose a technique for 3D fluid motion estimation applied to 3D-PIV. The most widely used technique for motion estimation in 2D-PIV is based on local correlation between two rectangular regions of the two images (see for instance [7]). This technique has a straightforward extension to 3D images. Another approach to motion estimation widely used in optical flow is a variational approach based on an energy minimization where on the one hand, we assume the conservation of the intensity of the displaced objects (in our case the particles) and on the other hand, we assume a certain regularity of the obtained flow. A variational approach was proposed in [4] in the context of 2D PIV. We propose to compare and combine both approaches in order to improve the accuracy of the flow estimation. The proposed method is very general and can be used in many applications of 3D flow estimation.

The paper is organized as follows: in section 2, we briefly describe the motion estimation using local cross-correlation; in section 3, we describe our variational approach; in section 4, we present the numerical experiments followed by the conclusion.

R. Moreno-Díaz et al. (Eds.): EUROCAST 2007, LNCS 4739, pp. 612–620, 2007.

2 Motion Estimation Using Local Cross-Correlation

Cross-correlation is the most common technique for fluid motion estimation in PIV and is described, for instance, in [6]. We will denote I_1 and I_2 the two images from which we compute the motion $\mathbf{u}$, N the image dimension (in our case $N = 3$) and Ω the domain of definition of the images.

2.1 Basic Principle

Having the two volumes I_1 and I_2, for each voxel $\mathbf{v} = (v_x, v_y, v_z)$ of I_1, the method takes a rectangular subvolume $I_{1,\mathbf{v}}$ of I_1 centered on $\mathbf{v}$, and looks for a similar subvolume of I_2 centered on a neighbor $\mathbf{v} + \mathbf{d}$ of $\mathbf{v}$. The similarity measure between two rectangular subvolumes of the same dimensions is based on 2D cross-correlation and is defined as:

$$C_{\mathbf{v}}(I_1, I_2)(\mathbf{d}) = \sum_{\mathbf{y}=(-a,-b,-c)}^{(a,b,c)} I_1(\mathbf{v}+\mathbf{y})\ I_2(\mathbf{v}+\mathbf{d}+\mathbf{y}) \tag{1}$$

The voxel $\mathbf{v}$ is assigned the displacement $\mathbf{d}$ which gives the maximal value of the cross-correlation. Doing this for every voxel we obtain a complete vector field $\mathbf{u}$.

2.2 Implementation Using Fast Fourier Transform

Because the process of computing the cross-correlation for many subvolumes of I_2 and for each voxel is computationally heavy, the implementation takes advantage of the properties of the Fourier transform to improve the processing time. The Fourier transform has the property that a correlation in the spatial domain is equivalent to a multiplication in the Fourier domain.

$$C_{\mathbf{v}}(I_1, I_2) = \mathcal{F}^{-1}(\widehat{I_{1,\mathbf{v}}}\ \widehat{I_{2,\mathbf{v}}}^{*}), \tag{2}$$

where $I_{1,\mathbf{v}}$ is a rectangular subvolume of I_1 centered on the voxel $\mathbf{v}$, $\widehat{I_{1,\mathbf{v}}}$ is the Fourier Transform of the subvolume $I_{1,\mathbf{v}}$, the operator * denotes the complex conjugate, and $\mathcal{F}^{-1}$ denotes the inverse Fourier transform. The image $C_{\mathbf{v}}(I_1, I_2)(\mathbf{d})$ gives the result of cross-correlation for all displacements $\mathbf{d}$ and the maximal value is a best estimate of the local displacement. Because of the hypothesis of periodicity introduced by the Fourier Transform, the window is usually chosen four times bigger than the expected displacement. The method is then extended to allow subvoxel accuracy by means of local interpolation of a Gaussian function close to the discrete maximum. When the correlation has been computed for every voxel, some kind of data validation procedure is needed to remove outliers.

The whole process should be applied iteratively a few times using the current result as an initialization for the next iteration. The iterative process can be initialized with a null vector field $\mathbf{u}^0 = 0$, and $\mathbf{u}^{n+1}$ can be estimated at each voxel of the lattice using the displacement with maximal correlation for a window of I_2 displaced by $\mathbf{u}^n$:

$$C_{\mathbf{v}}(I_1, I_2, \mathbf{u}^n) = \mathcal{F}^{-1}(\widehat{I_{1,\mathbf{v}}}\ \widehat{I_{2,\mathbf{v}+\mathbf{u}^n(\mathbf{v})}}^{*}), \tag{3}$$

By doing this, we can improve the accuracy of the fluid motion estimation. It also permits the progressive reduction of the size of the correlation window.

3 Variational Approach

Variational approach to motion estimation are often used for optical flow computation [5,3,2]. It consists in minimizing an energy as a function of the displacement and that depends on a pair of images I_1 and I_2.

In this section, E will denote the energy functional to minimize. For a given 3D vector field $\mathbf{u} = (u^x, u^y, u^z)^t$, the norm of its gradient $\| \nabla \mathbf{u} \|$ is defined as $\sqrt{\| \nabla u^x \|^2 + \| \nabla u^y \|^2 + \| \nabla u^z \|^2}$, and the Laplacian $\Delta \mathbf{u} = div(\nabla \mathbf{u})$ is defined as $(\Delta u^x, \Delta u^y, \Delta u^z)^t$.

The energy to minimize is expressed as :

$$E(\mathbf{u}) = \underbrace{\int_\Omega \left(I_1(\mathbf{x}) - I_2\left(\mathbf{x} + \mathbf{u}(\mathbf{x})\right)\right)^2 d\mathbf{x}}_{data\ term} + \underbrace{\alpha \int_\Omega \|\nabla \mathbf{u}(\mathbf{x})\|^2 d\mathbf{x}}_{regularization\ term}, \tag{4}$$

where α is a scalar coefficient that weights the smoothing term. Under the assumption of intensity conservation for each voxel, the first term (*data term*) becomes zero when the first image matches the second one displaced by $\mathbf{u}$: $I_1(\mathbf{x}) = I_2(\mathbf{x} + \mathbf{u}(\mathbf{x}))$. This term tries to find the vector field that best fits the solution. The second term is a *regularization term* which smoothes the vector field. There are a lot of ways to define the regularization term, including, for instance, discontinuities preserving constraints, etc. Since we deal with rather smooth flows, we have used the simplest regularity term presented above.

Euler-Lagrange equations yield:

$$(I_1(\mathbf{x}) - I_2(\mathbf{x} + \mathbf{u})).\nabla I_2(\mathbf{x} + \mathbf{u}) + \alpha div(\nabla \mathbf{u}) = 0 \tag{5}$$

3.1 Numerical Scheme

We propose to look for the minimum of the energy by solving (5) directly using a fixed point approach. An alternative is to use a gradient descent with either explicit or semi-implicit scheme. We use an iterative method to find $\mathbf{u}$:

$$\begin{cases} \mathbf{u}^0 & = \mathbf{u_0} \\ \mathbf{u}^{n+1} & = \mathbf{u}^n + \mathbf{h}^{n+1} \end{cases} \tag{6}$$

where we update the vector field $\mathbf{u}$ at each iteration by adding another vector field $\mathbf{h}$ with small displacements. The displacement $\mathbf{h}$ being small, we can use first order Taylor expansions of I_2 and ∇I_2 at $\mathbf{x} + \mathbf{u}^n$ to linearize (5):

$$d\mathbf{g} - \left[\mathbf{g}\mathbf{g}^t - dH'\right] \mathbf{h} + \alpha div(\nabla \mathbf{u}^n + \nabla \mathbf{h}) = 0 \tag{7}$$

denoting:

$$\mathbf{g}(\mathbf{x}) = \nabla I_2(\mathbf{x} + \mathbf{u}^n) \tag{8}$$

$$d(\mathbf{x}) = I_1(\mathbf{x}) - I_2(\mathbf{x} + \mathbf{u}^n) \tag{9}$$

$$H'(\mathbf{x}) = H(I_2)(\mathbf{x} + \mathbf{u}^n). \tag{10}$$

In the last equality, $H(I_2)(\mathbf{x})$ denotes the Hessian matrix of I_2 at the location $\mathbf{x}$. The term in second order spatial derivatives is usually neglected, supposing that the image varies slowly. Then, (7) becomes:

$$d\mathbf{g} + \alpha div(\nabla \mathbf{u}^n) - \mathbf{g}\mathbf{g}^t\mathbf{h} + \alpha div(\nabla \mathbf{h}) = 0 \tag{11}$$

After discretization using finite differences, the operator $div(\nabla \mathbf{h})$ can be divided in two terms $-2N\, I\, \mathbf{h}$ and $S(\mathbf{h})$, where the N is the image dimension and I is the identity matrix. The first term only depends on values of $\mathbf{h}$ at the current position $\mathbf{x}$ and the second term only depends on values of $\mathbf{h}$ at neighbor positions of $\mathbf{x}$: the vector $S(\mathbf{h})$ is written:

$$S(\mathbf{h}) = \begin{pmatrix} \sum_{\mathbf{y} \in N^*(\mathbf{x})} h^x(\mathbf{y}) \\ \sum_{\mathbf{y} \in N^*(\mathbf{x})} h^y(\mathbf{y}) \\ \sum_{\mathbf{y} \in N^*(\mathbf{x})} h^z(\mathbf{y}) \end{pmatrix}, \tag{12}$$

where $N^*(\mathbf{x})$ denotes the direct neighbors of $\mathbf{x}$ (4 in 2D and 6 in 3D), and $\mathbf{h} = (h^x, h^y, h^z)^t$.

Using $\mathbf{h}^{n+1}$ for the current location $\mathbf{x}$ and $\mathbf{h}^n$ for its neighbors, (11) becomes $A\mathbf{h}^{n+1} = b$, with $A = \mathbf{g}\mathbf{g}^t + \alpha 2N\, I$, and $b = d\mathbf{g} + \alpha div(\nabla \mathbf{u}^n) + S(\mathbf{h}^n)$. The matrix A is real, symmetric and positive definite, so it can be inverted and we can compute for each position $\mathbf{x}$, $\mathbf{h}^{n+1} = A^{-1}b$. To improve the convergence rate, we use a Gauss-Seidel method which updates the displacement $\mathbf{h}^{n+1}$ at position $\mathbf{x}$ using the values of $\mathbf{h}^{n+1}$ already calculated. This scheme is recursive and to avoid privileging the direction of scanning the image, we apply two successive iterations of Gauss-Seidel in reverse directions. Furthermore, we use a pyramidal approach to compute the displacement flow at several scales, using the results from a given scale to initialize to the following higher scale.

4 Experiments and Results

In this section, we present experiments on synthetic data using both methods (correlation and variational). We used a 3D flow based on realistic flow models to check the performance of the proposed methods. In these experiments, we first apply the correlation method to obtain a good approximation of the flow and then we refine the results with the variational approach.

4.1 Choice of the Parameters

The cross-correlation parameters are the window size in each dimension and the lattice spacing. The window size is approximately set to four times the expected

maximal displacement and is the same in each dimension. In the following experiments, we use a lattice spacing of 2 voxels in each dimension, and the final result is interpolated to obtain a dense estimation. The variational approach uses the parameters of α and the number of scales for the pyramidal approach. In the following experiments, we will show the sensitivity of the method to the regularization coefficient α and we will choose the value that gives best results.

4.2 Description of the Models

In the first model we use an incompressible 3D flow model suggested to us by Professor Scarano that can be found in [9] (section 3-9.2). It corresponds to the Stokes's solution for an immersed sphere. The flow moves in the horizontal axis direction with a velocity $(U, 0, 0)$, and it avoids the sphere located at the center of the volume. The flow inside the sphere is null.

The second model has been suggested to us by the CEMAGREF Institute and it has been obtained using a Large Eddy Simulation of the incompressible Navier-Stokes equations which defines the turbulent motion after a cylinder. It simulates a volume with synthetic particles following the horizontal axis and a cylinder situated on the z-axis obstructing the flow perpendicularly. We use two successive images from this sequence. The original model is a volume of 960 x 960 x 144 voxels but we limit our experiment to a window of 256 x 64 x 64 voxels to reduce the computation time. This window includes part of the cylinder and the turbulence behind it.

4.3 Experiments with Model 1 (Sphere)

Table 1 shows the best average error and standard deviation reached for each method individually and their combination. The correlation was applied 11 times with a window size of 8 voxels. The individual variational approach was applied using 3 scales and $\alpha = 8.4$. Finally, the combined method used the correlation result as an initialization for the variational method, applied with $\alpha = 1.1$ and one scale. The standard deviation is always about the same order as the average error, and although the variational and the cross-correlation methods reaches similar accuracies, combining them brings the error almost to half. Figure 1 (right) shows the final average error distribution using the combined scheme. We can observe that the highest error is located at the sphere boundaries.

The left curve in Figure 2 displays the average error evolution using the combined scheme. First, we apply 11 iterations of correlation technique. Next, we use the output flow provided by the correlation as the input flow of the variational technique (curve after iteration 11). We observe a significative improvement in the flow estimation error after using the variational method. The right curve depicts the average error for different values of α using the variational approach initialized with the best correlation result. The minimal average error (0.0138 voxel) is obtained for $\alpha = 1.1$.

Table 1. Comparison between the two methods for the different models

Model 1	**Correlation**	**Variational**	**Cor.+Var.**
av. error	0.0272	0.0245	0.0138
std. dev.	0.0275	0.0230	0.0169
Model 2	**Correlation**	**Variational**	**Cor.+Var.**
av. error	0.1673	0.0954	0.0694
std. dev.	0.1337	0.0849	0.0756

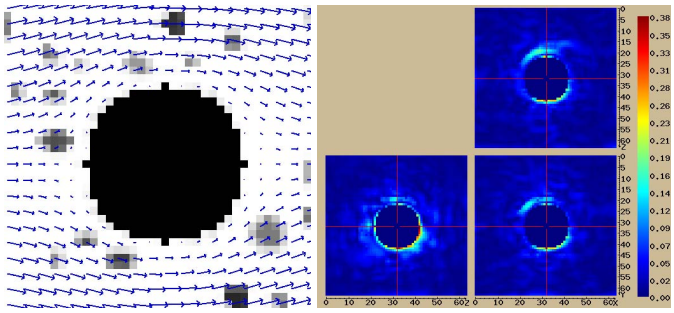

Fig. 1. Left, real flow (with zoom). Right, final error distribution (combined scheme).

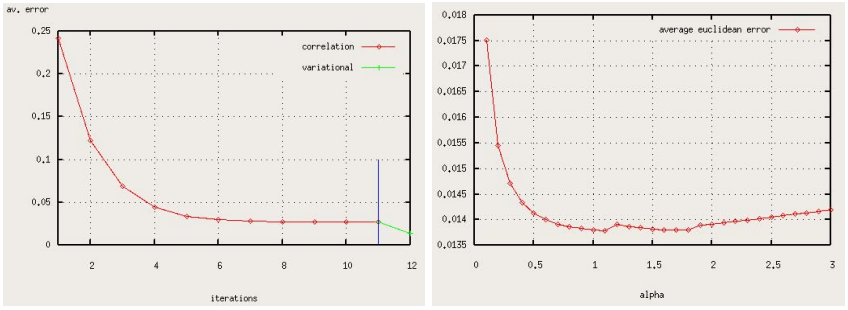

Fig. 2. Left, average error evolution using the combined scheme (11 times cor.+ var.). Right, average error depending on α for the combined approach.

4.4 Experiments with Model 2 (Cylinder)

We ran the same kind of experiments for this model as for the previous one. Table 1 shows the best average error and standard deviation reached for each method individually and their combination. The correlation was applied 6 times with a sequence of different window sizes: 16, 16, 8, 8, 4, 4. The variational approach was applied using $\alpha = 3.7$ and 3 scales. Finally, the combined method used the correlation result as an initialization for the variational method, applied with

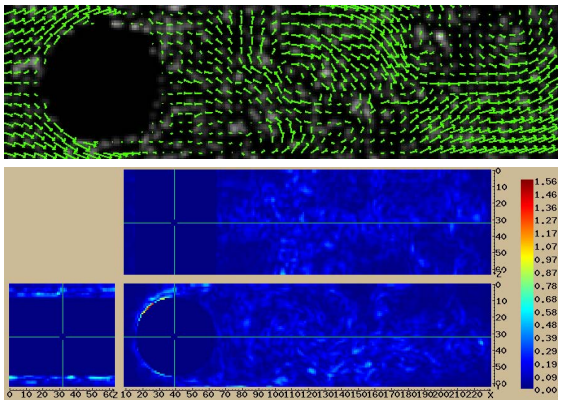

Fig. 3. Top, real flow. Bottom, final error distribution (combined scheme).

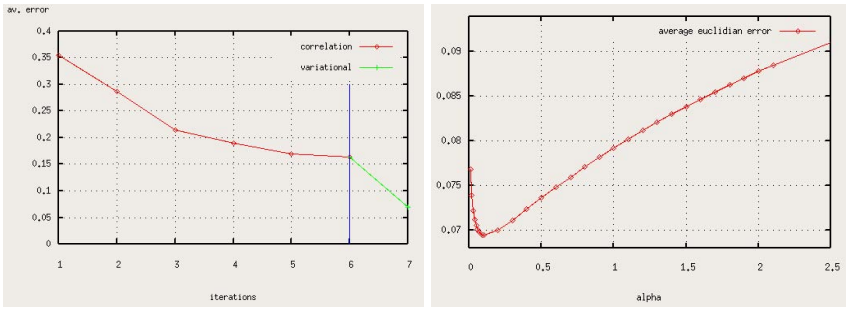

Fig. 4. Left, average error evolution using the combined scheme (6 times cor.+var.). Right, average error depending on α for the combined approach.

α=0.1 and one scale. The standard deviation is about the same order as the average error. In this experiment, the variational method reaches a better result than the correlation, and their combination still brings a substantial improvement. Figure 3 (right) shows the final average error distribution using the combined scheme. As in the previous model, the highest error is also located at the obstacle boundaries.

5 Conclusion

In this paper, we presented a 3D flow estimation technique based on the combination of correlation and variational methods. We have implemented both techniques and we have shown in the numerical experiments that a combination of both methods (using the output of the correlation technique as the initial

input of the variational method) improves the accuracy of the flow estimation. Indeed, several iterations of the cross-correlation technique followed by single scale variational approach gave us the best results in both images with a substantial improvement. This result can be interpreted in the following way: although the variational method is minimizing a global energy, it can only find a local minimum with a small displacement. Thus, the correlation technique gives the variational method a better initialization than the pyramidal approach.

Although we focused our attention to 3D fluid flow analysis, the proposed methodology is very general and can be applied to different application fields. Correlation based techniques and energy minimization techniques have been developed in the research community in a completely independent way. Each one has its own advantages and limitations but we think that an adequate combination of both can improve the global estimation of the flow.

In future work, we plan to investigate other regularization terms as proposed in [8,1]. We also think that including physical 3D flow constraints, as for instance the incompressibility, to the 3D flow estimation, is a very important issue that allows combining the mathematical models of fluid motion with the experimental data. We plan to compare our current method with approaches which include an incompressibility constraint within the variational formulation [4,10] and also apply solenoidal projections to make our results divergence free.

Acknowledgments

This work has been funded by the European Commission under the Specific Targeted Research Project FLUID (contract no. FP6-513663). We acknowledge the Research Institute CEMAGREF (France) for providing to us the PIV sequence we have used in the experiments.

References

1. Alvarez, L., Weickert, J., Sánchez, J.: Reliable estimation of dense optical flow fields with large displacements. International Journal of Computer Vision 39(1), 41–56 (2000)
2. Barron, J.L., Fleet, D.J., Beauchemin, S.S.: Performance of optical flow techniques. IJCV 12(1), 43–77 (1994)
3. Beauchemin, S.S., Barron, J.L.: The computation of optical flow. ACM Computing Surveys 27(3), 433–467 (1995)
4. Corpetti, T., Heitz, D., Arroyo, G., Mémin, E., Santa-Cruz, A.: Fluid experimental flow estimation based on an optical-flow scheme. Experiments in Fluids 40(1), 80–97 (2006)
5. Horn, B., Schunck, B.: Determining optical flow. MIT Aritificial Intelligence Laboratory (April 1980)
6. Raffel, M., Willert, C., Kompenhans, J.: Particle Image Velocimetry. A Practical Guide. Springer, Heidelberg (1998)
7. Scarano, F.: Iterative image deformation methods in piv. Measc. Sci. Technol. 13, R1–R19 (2002)

8. Weicker, J., Schnorr, C.: A theoretical framework for convex regularizers in pde-based computation of image motion. International Journal of Computer Vision 45(3), 245–264 (2001)
9. White, F.: Viscous Fluid Flow. McGraw-Hill, New York (2006)
10. Yuan, J., Ruhnau, P., Memin, E., Schnörr, C.: Discrete orthogonal decomposition and variational fluid flow estimation. In: Kimmel, R., Sochen, N.A., Weickert, J. (eds.) Scale-Space 2005. LNCS, vol. 3459, pp. 267–278. Springer, Heidelberg (2005)